Program Digest, 2019 IEEE International Ultrasonics Symposium (IUS)
Glasgow, Scotland, October 6-9, 2019

Minimum Variance beamforming for closely spaced microbubbles

Konstantinos Diamantis
Institute for Digital Communications
University of Edinburgh
Edinburgh, UK
K.Diamantis@ed.ac.uk

Mairead Butler
School of Engineering and Physical Sciences
Heriot-Watt University
Edinburgh, UK
M.Butler@hw.ac.uk

Tom Anderson
Centre for Cardiovascular Science
The University of Edinburgh
Edinburgh, UK
tanders1@exseed.ed.ac.uk

Jørgen Arendt Jensen
Center for Fast Ultrasound Imaging
Technical University of Denmark
Lyngby, Denmark
jaj@elektro.dtu.dk

Vassilis Sboros
School of Engineering and Physical Sciences
Heriot-Watt University
Edinburgh, UK
V.Sboros@hw.ac.uk

***Abstract*— The Minimum Variance beamformer (MVB) is known to outperform the conventional Delay-and-Sum (DAS) beamformer in terms of lateral resolution. Super-resolution ultrasound imaging (SRI) relies on localising several microbubbles in each image, and thus the objective of this work is to assess how the distance between two scatterers can affect their apparent size or shape on the image by using the MVB. The MVB method was employed on simulated point scatter data with a 8 MHz (λ=192 μm) 128-element linear array probe. Two scatterers were placed in variable positions in three dimensions and closely spaced to each other. The lateral Full-Width-Half-Maximum (FWHM) was used for performance evaluation. It was found that the FWHM of each scatterer was affected by the presence of another, and decreased as the distance between two scatterers increased. Relative positioning in axial (0.1mm apart) or azimuthal (1 mm apart) positions provided a tilted scatterer appearance. As the MVB differentiates scatterers at closer distances compared to the DAS beamformer, it is concluded that a larger number of microbubbles can be counted using the former.**

Keywords—microbubble, beamformer, super-resolution, minimum variance, delay-and-sum

I. Introduction

Ultrasonic sensor signals are processed conventionally using the delay-and-sum (DAS) beamformer. Boxcar, Hanning or Hamming window functions are typically employed as weighting functions regardless of the data type. This procedure is tailored to structural/anatomical imaging, where the objective is to visualize large internal body organs. The DAS beamforming does not favour the detection and localisation of point scatterers such as ultrasound contrast microbubbles (MBs) [1]. In order to resolve this, instead of fixed functions, adaptive weights may be calculated for each signal point.

The objective is to ensure unity gain for a signal location while suppressing contributions from other locations. A number of studies have shown that the adaptive method can provide more than 10 fold lateral resolution improvements compared to DAS [2]-[5]. The objective of this work is to determine the appearance of scatter for closely spaced scatterers and determine whether the higher resolution yielded by the MVB is maintained. This is investigated here by performing a Field II [6, 7] simulation study.

II. Methods

The time-domain implementation of the MVB has been described with detail in [2,4,8]. An 8 MHz linear array consisting of 128 elements was employed to scan a number of simulated Field II point scatterers positioned between (x, z) = (0 mm, 40 mm) and (x, z) = (0 mm, 100 mm), with an axial step of 10 mm. The speed of sound, c, was set to 1540 m/s, with wavelength λ = 192.5 μm. The sampling frequency was 100 MHz. Two point scatterers at 70 mm depth were simulated and subsequently scanned. They were separated laterally by 400 μm (~2λ). A single spherical wave was emitted for each scan using 64 transducer elements. The virtual source was positioned behind the transducer central element [9]. The excitation function was an 8-cycle sinusoid at 8 MHz, weighted by a 50% Tukey window.

The RF data from each emission were acquired from all elements individually in receive. The MVB was then used to beamform a single emission image, by calculating an adaptive weight for each pixel.

This work was supported by the Science and Technology Facilities Council (STFC-ST/M007804/1).

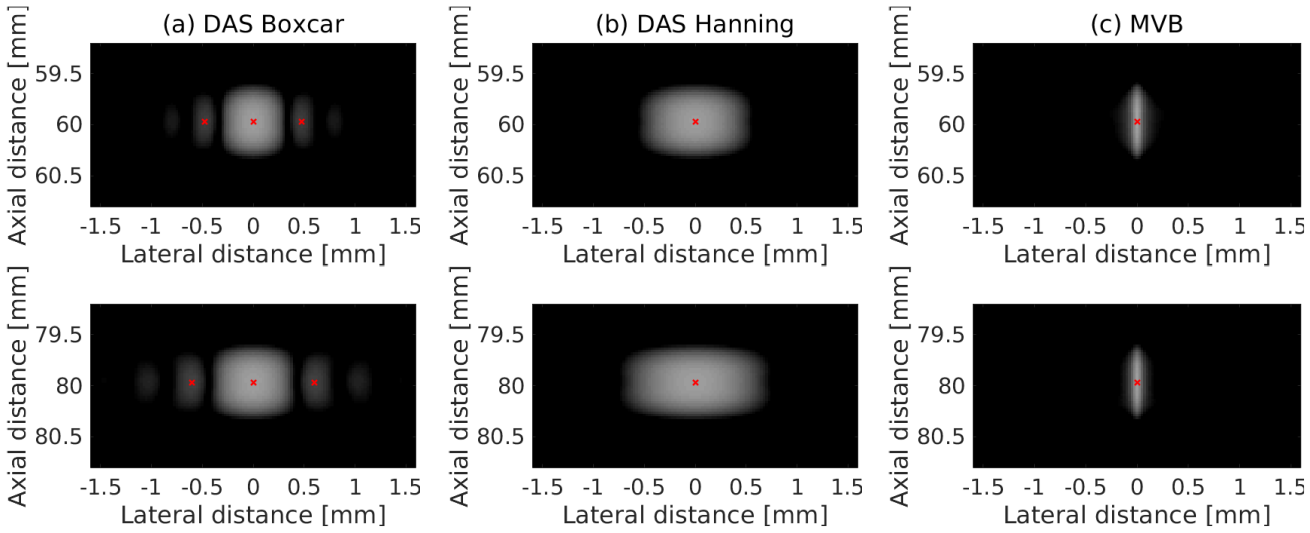

Fig 1 Beamformed responses of a Field II simulated scatterer at 60 mm (1st row) and 80 mm (2nd row) depth with (a) DAS Boxcar, (b) DAS Hanning, (c) MVB apodization. The dynamic range of the display was 40dB

A sub-array length, L≈2M/3 = 80 was employed as in [5]. Furthermore, fixed Boxcar and Hanning weights were also applied to all simulated data to form DAS beamformed images for comparison. The Full Width Half Maximum (FWHM) was used as means to assess resolution.

III. Results and Discussion

Fig. 1 shows two examples of the beamformed responses of single scatterers at 60 mm and 80 mm depths. At 60 mm depth, the lowest lateral FWHM value was 74.8 μm (or 0.39λ) and was achieved by the MVB. The equivalent FWHM values corresponding to DAS Boxcar and Hanning, were 400 μm (or 2.08λ) and 633.9 μm (or 3.29λ) respectively. The power in dB (y-axis) for the different lateral positions (x-axis) at 60 mm depth can be found for all beamformers in Fig. 2.

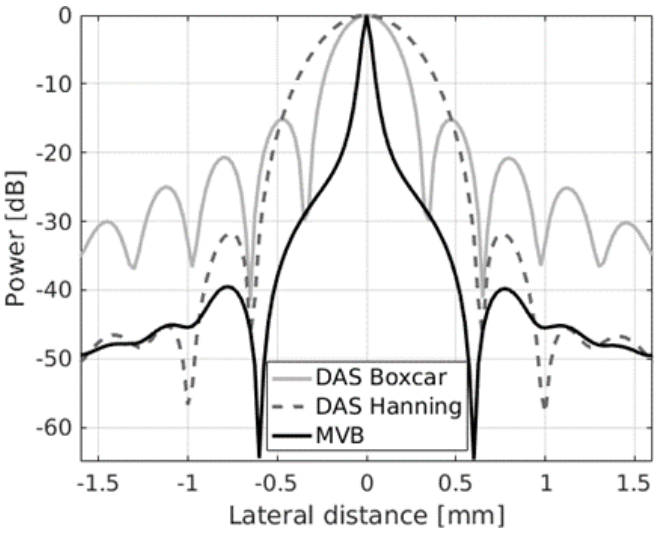

Fig. 2 Lateral power variations at 60mm depth for beamformed responses of the single scatterer displayed in Fig 1 (1st row).

At 80 mm depth, the FWHM was measured to be 74.1μm (or 0.38λ) from the MVB response. The measured FWHM values using the conventional beamformers were 514.3 μm (or 2.67λ) and 830.2 μm (or 4.31λ) for Boxcar and Hanning weights respectively. In general the measured FWHM was fairly constant using the MVB for the entire depth range studied here (40 mm-100 mm) and only varied between 71.9 μm (or 0.37λ) and 99.2 μm (or 0.52λ). On the other hand, the measured FWHM using the DAS beamformers increased monotonically with depth due to the fixed receive aperture used. Therefore, the FWHM values obtained by the DAS Boxcar ranged between 301.6 μm (or 1.57λ) and 633.3 μm (or 3.29λ). Finally DAS Hanning resulted in lateral FWHM values between 451 μm (or 2.34λ) and 1028 μm (or 0.52λ).

Fig. 3 shows the beamformed responses of a simulated pair of scatterers at 70 mm depth. The two scatterers were positioned at (x,z) = (±0.2 mm, 70 mm). Fig. 3 (a)-(b) shows that the two scatterers appear merged when using the conventional beamformers for image formation. The measured lateral FWHM was 684.2 μm (or 3.55λ) and 877.2 μm (or 4.56λ) for DAS Boxcar and DAS Hanning respectively. Importantly the side-lobes in the DAS Boxcar beamformed response were significantly lower than in Fig. 1(a) and not visible, which was also confirmed by the lateral variations displayed in Fig. 4. By contrast, two scatterers were identified in the MVB case as shown in Fig. 3 and confirmed by the presence of two peaks in the power variations at 70 mm depth for all lateral positions (Fig.4). The lateral FWHM for each of the two scatterers was measured to be 227.1 μm (or 1.18λ). The two scatterers could be distinguished with 350 μm (≈1.8λ) and 575 μm (≈ 3.0λ) between them for the MVB and the DAS beamformers, while

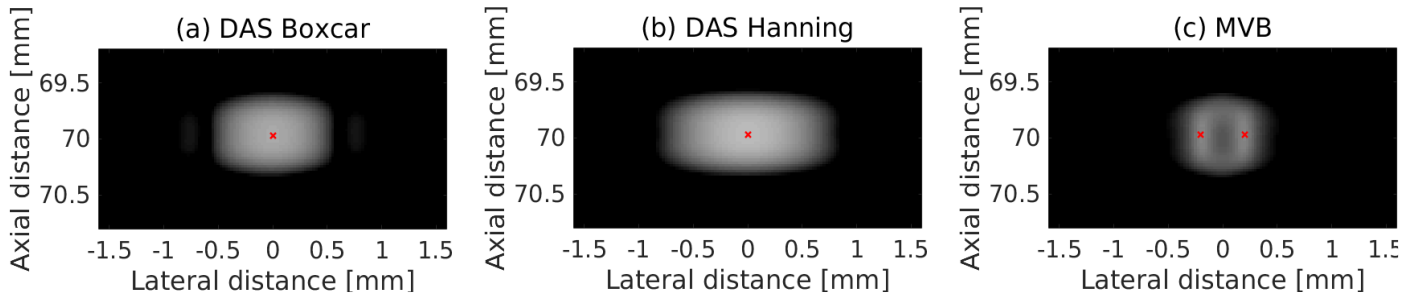

Fig. 3 Beamformed response of two Field II simulated scatterers at 70 mm depth with (a) DAS boxcar, (b) DAS hanning, (c) MVB apodization. The dynamic range of the display was 40dB.

they appeared as a single scatterer at shorter respective distances. The FWHM of each scatterer was affected by the presence of another, and decreased as the distance between two scatterers increased. The FWHM eventually converged to that of single scatter at distances of several wavelengths. This is attributed to the interaction of the main lobes of the scatterers.

In addition, relative positioning in axial (0.1mm apart) or azimuthal (1 mm apart) positions provided a tilted scatterer appearance, which is due to the lack of symmetry in the interaction of the main lobes of the scatterers. As the MVB differentiates scatterers at closer distances compared to the DAS beamformer, it is concluded that a larger number of microbubbles can be counted using the former. This strongly suggests that more paths and thus microvessels would be possible to resolve using the MVB.

The use of the adaptive beamformer is relevant to the emerging field of super-resolution ultrasound, that aims to increase image resolution by the precise localisation of individual MBs [10]-[14] which are efficient point scatterers. At present, most super-resolution methods are based on image processing and on DAS beamformed images, and depend on localisation algorithms for the determination of position. The cost of these lateral resolution gains using the MV beamformer, is the increased computational load [4]. This is due to the individual weight calculation, which involves the inversion of large matrices and computations between them. This can be dealt with off-line, with parallel computing using modern graphics processing units (GPUs) as in [15], and should not be confused with the data acquisition rate. The latter can be extremely high due to the formation of single emission beamformed responses. The results presented in this work suggest that the MVB may be well-suited to the localisation and detection of MBs.

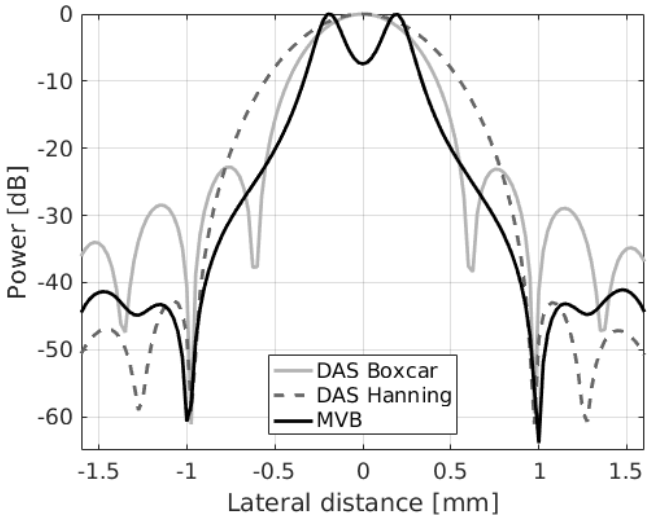

Fig. 4 Lateral power variations at 70 mm depth for beamformed responses of the two scatterers displayed in Fig. 3.

IV. Conclusion

The Minimum Variance beamformer (MVB) provides improved resolution compared to the conventional delay-and-sum (DAS) beamformers for the case of closely spaced scatterers. However, the scatter vicinity affect the appearance of each scatterer in terms of size and shape. These results show that the adaptive beamformer has the potential to achieve improved resolution compared to conventional beamforming by means of localising an increased number of scatterers. This may prove advantageous to ultrasound super-resolution imaging.

References

[1] V. Sboros, C. M. Moran, S. D. Pye, and W. N. McDicken, "The behaviour of individual contrast agent microbubbles," *Ultr. Med. Biol.*, vol. 29, no. 5, pp. 687–694, 2003.

[2] J. F. Synnevåg, A. Austeng, and S. Holm, "Adaptive beamforming applied to medical ultrasound imaging," *IEEE Trans. Ultrason., Fer- roelectr., Freq. Control*, vol. 54, no. 8, pp. 1606–1613, Aug. 2007.

[3] I. K. Holfort, F. Gran, and J. A. Jensen, "Broadband minimum variance beamforming for ultrasound imaging," *IEEE Trans. Ultrason., Ferro- electr., Freq. Control*, vol. 56, no. 2, pp. 314–325, Feb. 2009.

[4] K. Diamantis, I. H. Voxen, A. H. Greenaway, T. Anderson, J. A. Jensen, and V. Sboros, "A comparison between temporal and subband minimum variance adaptive beamforming," in *Proc. SPIE Med. Imag.*, vol. 90400L, Mar. 2014. [Online]. Available: 10.1117/12.2043602.

[5] K. Diamantis, A. Greenaway, T. Anderson, J. A. Jensen, and V. Sboros, "Experimental performance assessment of the sub-band minimum vari- ance beamformer for ultrasound imaging,"

Ultrasonics, vol. 79, pp. 87– 95, 2017.

[6] J. A. Jensen and N. B. Svendsen, "Calculation of pressure fields from arbitrarily shaped, apodized, and excited ultrasound transducers," *IEEE Trans. Ultrason., Ferroelectr., Freq. Control*, vol. 39, pp. 262–267, 1992.

[7] J. A. Jensen, "Field: A program for simulating ultrasound systems," *Med. Biol. Eng. Comp., vol. 10th Nordic-Baltic Conference on Biomedical Imaging Supplement 1, Part 1*, vol. 4, pp. 351–353, 1996.

[8] K. Diamantis, T. Anderson, M.B. Butler, C.A. Villagomez-Hoyos, J.A. Jensen, and V. Sboros, Resolving Ultrasound Contrast Microbubbles using Minimum Variance Beamforming. *IEEE Transactions on Medical Imaging* vol 38 pp 194-204, 2019

[9] N. Oddershede and J. A. Jensen, "Effects influencing focusing in syn- thetic aperture vector flow imaging," *IEEE Trans. Ultrason., Ferroelectr., Freq. Control*, vol. 54, no. 9, pp. 1811–1825, September 2007.

[10] M. A. O'Reilly, R. M. Jones, and K. Hynynen, "Three-dimensional transcranial ultrasound imaging of microbubble clouds using a sparse hemispherical array," *IEEE Trans. Biom. Eng.*, vol. 61, no. 4, pp. 1285– 1294, 2014.

[11] K. Christensen-Jeffries, R. J. Browning, M. X. Tang, C. Dunsby, and R. J. Eckersley, "*In vivo* acoustic super-resolution and super-resolved velocity mapping using microbubbles," *IEEE Trans. Medical Imaging*, vol. 34, no. 2, pp. 433–440, Feb. 2015.

[12] C. Errico, B. F. Osmanski, S. Pezet, O. Couture, Z. Lenkei, and M. Tanter, "Transcranial functional ultrasound imaging of the brain using microbubble-enhanced ultrasensitive Doppler," *NeuroImage*, vol. 124, no. Pt A, pp. 752–761, 2015.

[13] D. Ackermann and G. Schmitz, "Detection and tracking of multiple microbubbles in ultrasound b-mode images," *IEEE Trans. Ultrason., Ferroelec., Freq. Contr.*, vol. 63, no. 1, pp. 72–82, Jan. 2016.

[14] K. B. Hansen, C. A. Villagmez-Hoyos, J. C. Brasen, K. Diamantis, I. Sboros, C. M. Srensen, and J. A. Jensen, "Robust microbubble tracking for super resolution imaging in ultrasound," in *Proc. IEEE Ultrason. Symp.*, Sept 2016, pp. 1–4.

[15] J. P. Asen, J. I. Buskenes, C. I. C. Nilsen, A. Austeng, and S. Holm, "Implementing Capon beamforming on a GPU for real-time cardiac ultrasound imaging," *IEEE Trans. Ultrason., Ferroelectr., Freq. Control*, vol. 61, no. 1, pp. 76–85, Jan. 2014.